https://doi.org/10.26599/FRICT.2026.9441309

Research Article

Robust insensitivity of heterogeneous charge distribution and interlayer friction to strong external electric fields in twisted graphene bilayers

Hao Li, Wanlin Guo and Yufeng Guo✉

State Key Laboratory of Mechanics and Control for Aerospace Structures, MOE Key Laboratory for Intelligent Nano Materials and Devices, College of Aerospace Engineering, Nanjing University of Aeronautics and Astronautics, Nanjing 210016, China

✉ E-mail: yfguo@nuaa.edu.cn

Received: April 5, 2026; Revised: August 13, 2026; Accepted: September 2, 2026

Abstract: Twisted graphene bilayers exhibit rich physical phenomena under external fields, yet the coupled effect of electric fields and interlayer sliding on their charge distribution remains elusive. By combining first-principles calculations with a machine learning technique, we systematically investigate interlayer sliding-induced charge transfer and redistribution in both twisted and AB-stacked graphene bilayers under vertical electric fields. Unlike the homogeneous charge distribution observed in AB-stacked bilayers, the heterogeneous charge distribution in certain twisted graphene bilayers exhibits robust insensitivity to applied electric fields, even under strong fields up to 2 V/nm. This field

insensitivity enables such twisted bilayers to maintain ultralow interlayer friction under extreme bias conditions. To quantitatively describe the coupled effect of interlayer sliding and electric fields on interlayer charge transfer and friction, we develop a charge-modified registry index (RI_{CM}) model for graphene bilayers. The revealed electric-field insensitivity in specific twisted configurations can be mainly attributed to the inherently small variation in the maximum registry index change (ΔRI_{CM}) under bias, providing a simple descriptor for designing low-friction interfaces in electrically gated graphene devices.

Keywords: Twisted graphene bilayer, heterogeneous charge, electric-field insensitivity, friction, machine learning

1 Introduction

As an important member of the graphene family, graphene bilayers possess exceptional physical and mechanical properties, rendering them highly promising for applications in electronics[1], spintronics[2], and nanoelectromechanical systems[3]. When the top and bottom layers of an AB-stacked graphene bilayer are rotated or twisted in-plane relative to each other, an incommensurate structure emerges due to the resulting atomic registry mismatch between the two layers. This incommensurability can give rise to a moiré superlattice for twisted graphene bilayers, in which the electronic bandwidth can become comparable in energy to the Coulomb interactions [4]. Recent studies on magic-angle (~1.08°) twisted graphene bilayers have revealed various electronic states, including correlated insulators [5], superconductors [6], topological phases [7], and the formation of two nearly flat bands near charge neutrality [8]. Moreover, the incommensurability can lead to extremely low interfacial friction during the relative sliding of top and bottom layers of twisted graphene bilayers [9], as the interlayer interaction forces between atoms cancel out. Nevertheless, this

ultralow interlayer friction is highly sensitive to the degree of lattice commensurability between the two graphene layers and vanishes when one layer is rotated by a critical angle [10].

Applying a bias voltage to a graphene bilayer will induce charge transfer and exchange between graphene layers, representing an effective and widely adopted strategy for precisely tuning their physical properties. For instance, the application of a vertical electric field to an AB-stacked graphene bilayer can break its inversion symmetry and open up a bandgap in its energy spectrum, turning it from a semimetal into a semiconductor [11]. Chushan Li et al. reported the observation of superconductivity in electron- and hole-doped Bernal bilayer graphene under a high vertical electric field of 1.6 V/nm [12]. Beyond commensurate stacking, Chao-Hui Yeh et al. reported that the electron-hole symmetry in the low-energy band structure for a twisted graphene bilayer with a critical rotation angle can be effectively manipulated by applying a gate voltage [13]. More recently, an experimental study showed that the band structure tuning through an external electric field can influence the emergence of superconductivity in a near magic-angle twisted graphene bilayer, with superconductivity being suppressed at an electric field strength of 0.67 V/nm [14]. Experimentally, the maximum stable electric field strength achieved by applying a bias voltage on graphene bilayers without inducing electrical leakage or breakdown on dielectric layers or substrates is typically no higher than 2 V/nm. On the other hand, the charge transfer between AA/AB-stacked graphene layers induced by an applied bias voltage inevitably strengthens interlayer Coulomb interactions, thereby increases both interlayer coupling and friction [15,16]. Given the rapid development of electrically tunable functionalization in graphene based nanodevices, understanding their interface behavior under extreme and practically relevant bias conditions is essential. However, the impact of strong electric fields on the interlayer charge transfer and the tribological behavior of twisted graphene bilayers, as well as the role of the twist angle in governing charge distribution in the graphene layers, remain poorly understood and have rarely been systematically investigated.

In this study, charge transfer and redistribution in both twisted and AB-stacked graphene bilayers under the coupled influence of interlayer sliding and vertical electric fields have extensively been investigated using a density-functional-theory (DFT) based machine learning (ML) method. When the top and bottom layers of graphene bilayers undergo relative in-plane sliding, twisted bilayers display a spatially heterogeneous charge distribution, in contrast to the homogeneous charge distribution observed in AB-stacked bilayers. The charge deviations induced in C atoms of certain twisted configurations during interlayer sliding are highly insensitive to applied electric fields, even under a strong field of 2 V/nm. This field insensitive behavior maintains ultralow interlayer friction under strong fields and results in only minor changes in energy band gaps during interlayer sliding. A charge-modified registry index (RI_{CM}) model, incorporating the influence of electric fields and charge deviations in C atoms, is developed to quantitatively elucidate the relationship between field-induced charge redistribution and interlayer registry across the top and bottom graphene layers. In both the presence and absence of an electric field, the maximum charge change induced in the graphene layers by interlayer sliding exhibits a nonmonotonic dependence on twist angle, while increasing linearly with the corresponding maximum registry index change (ΔRI_{CM}). The robust insensitivity of interlayer charge transfer and friction to strong electric fields in specific twisted bilayers mainly stems from the inherently small variation in ΔRI_{CM} between biased and unbiased conditions.

2 Model and methods

Initially, an AB-stacked graphene bilayer was constructed in a rhombus unit cell as the initial structure, as shown in Fig. 1a. The top layer was subsequently rotated relative to the bottom layer about the *O* point by five distinct twist angles θ: 6.0°, 7.3°, 9.4°, 13.2°, and 21.8°. As shown in Fig. S1 in the Supplementary Material, five twisted graphene bilayers with different moiré superlattices were obtained. Periodic boundary conditions were applied in the a_1 and a_2 directions, with a vacuum region of 25 Å in the vertical direction. The lengths of the top graphene layers in the unit cells are identical to those of the bottom layers, and these twisted bilayers are strain-free. Details regarding unit cell sizes

and quantities of atoms are provided in Table S1 in the Supplementary Material. All DFT computations for the established bilayers were performed in the Vienna Ab-initio Simulation Package code (VASP) [17,18] by using the projector augmented wave method with the Perdew-Burke-Ernzerhof (PBE) exchange-correlation functional [18–20]. The influence of van der Waals (vdW) interactions was considered by using vdW-DF2 dispersion correction [21]. A plane wave energy cutoff was set to 500 eV, and a special Γ-centered *k* points sampled on a $5 \times 5 \times 1$ mesh was employed. All structures were relaxed by using a conjugate gradient algorithm until the forces on each atom were less than 0.01 eV/Å. Next, external electric fields with the field strengths of 1 and 2 V/nm were applied along the vertical direction, respectively, followed by full structural relaxation. Both applied electric field strengths, particularly the 2 V/nm field, are experimentally classified within the strong-field regime [1,21,22]. The applied electric fields impose a negligible influence on the equilibrium interlayer distances of these bilayers, see Fig. S4. To simulate the interlayer sliding in these bilayers, the in-plane unit cell was discretized into a 9×9 grid (81 equally spaced positions), and the top graphene layer was translated relative to the bottom layer and sequentially shifted to each of the predefined in-plane positions while maintaining the interlayer distance fixed. For a twisted or AB-stacked graphene bilayer, five distinct stacking configurations were randomly selected out from its 81 stacking positions for subsequent static DFT calculations. The obtained charge densities of these bilayers with selected stacking configurations both in the absence and presence of an electric field served as training sets (total 30 training sets) for next ML study.

A ML technique developed by Chandrasekaran et al. [23] was employed in our study to predict charge densities of graphene bilayers at the 81 stacking positions based solely on the positions of C atoms, which significantly reduces the substantial computational resources and time otherwise required by DFT calculations. This ML technique utilized scalar, vector, and tensor fingerprints as predictors of charge density, capturing diverse attributes of atomic neighborhoods that encompass features analogous to scalar, vector, and tensor quantities. The ML model was implemented using

Keras with TensorFlow as the backend, with mean squared error (MSE) as the loss function [24]. The model was trained using charge densities derived from DFT calculations. The ADAM stochastic optimization algorithm facilitated gradient descent [25]. The deep neural network (DNN) architecture [26] comprised three hidden layers, each containing 300 neurons, and utilized the Rectified Linear Unit (ReLU) activation function [27], as shown in Fig. 1b. Further details regarding the unit cell setup and ML model are provided in the Supplementary Material. The comparison of charge density prediction between the ML model and DFT for the six AB-stacked and twisted graphene bilayers is shown in Fig. 1c and d. The root mean square errors (RMSE) of the training and prediction sets are about 0.9% and 1.4%, respectively, ensuring the validity of the employed ML model in accurately predicting charge density. The ML model for bilayers under electric fields was separately trained by using the same procedure, see Fig. S3. Next, the charge densities of the six AB-stacked and twisted bilayers at the 81 stacking positions without and under electric fields were predicted by the DFT-based ML models, respectively.

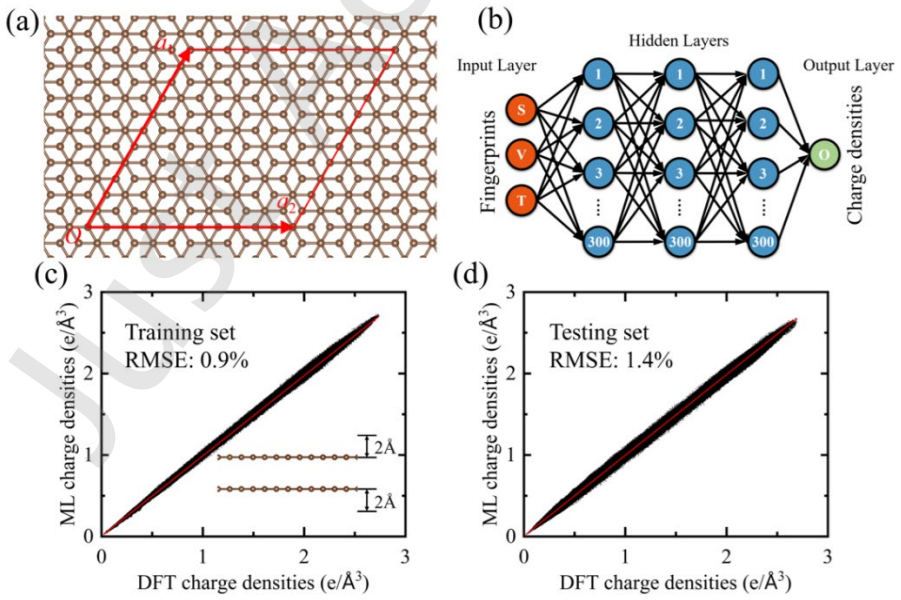

Fig. 1 (a) Top view of an AB-stacked graphene bilayer. The brown balls denote C atoms. (b) Detailed display of the employed DNN. (c) Parity plot of the ML vs DFT charge density prediction of six

graphene bilayers for a training dataset. The inset shows the sampling thickness of training set. (d) Parity plot of the ML vs DFT charge density prediction of six graphene bilayers for a testing dataset.

We have constructed additional twisted graphene bilayers by rotating the top layer of the AB-stacked bilayer at twist angles θ of 1.1°, 2.1°, 3.2°, 19.98°, 24.03°, 27.8°, 29.957°, 35.6°, 38.2°, 46.8° and 52.1°, respectively, as shown in Fig. S2. The lattice lengths of the top layers in these twisted bilayers match with those of the corresponding bottom layers. However, the quantities of atoms in these bilayers (see Table S2) far exceed the computational capability of present DFT calculation. Consequently, structural relaxation of these twisted bilayers was performed using the adaptive intermolecular reactive empirical bond order (AIREBO) potential [28], as implemented in the LAMMPS software package. The interlayer vdW interactions between C atoms were described by a 6-12 Lennard-Jones (LJ) potential. By performing the same interlayer sliding setting, the charge densities of these twisted bilayers at the 81 stacking positions without and under electric fields were predicted by the DFT-based ML models, respectively.

3 Results and Discussion

Bader charge partitions the continuous electron density via zero-flux surfaces and integrates the density within each atomic basin, thereby preserving the essential charge transfer information at the interface in a discrete yet physically faithful manner [29]. Based on the ML predicted charge densities, the Bader charge deviations Δq_i of each C atom in these bilayers with respect to the C atoms of free-standing monolayers both in the absence of and under electric fields were calculated for all stacking positions. A positive Δq_i means charge depletion, whereas a negative value means charge accumulation. The Bader charge deviations in C atoms can exactly reflect the coupled influence of interlayer sliding and electric field on the interlayer charge transfer and exchange between the top and bottom graphene layers. Then the total charge deviation q_t in the top layer at a stacking position was calculated by $q_t = \sum_{i=1}^{n} \Delta q_i / S$, where n represents the number of C atoms in the top layer and S is the in-plane area of the unit cell. Meanwhile, the total charge deviation in the bottom layer is $-q_t$ owing to global charge

conservation. According to the calculated total charge deviations q_t at the 81 stacking positions, the total charge deviation surfaces (TCDSs) of the top and bottom layers under interlayer sliding were derived for all considered AB-stacked and twisted bilayers. As shown in Figs. S5-7, there are maximum and minimum q_t (defined as q_t^{max} and q_t^{min}, respectively) in the top layers at specific stacking positions, at which there correspondingly are $-q_t^{max}$ and $-q_t^{min}$ in the bottom layers. The stacking configurations corresponding to q_t^{max} and q_t^{min} for all graphene bilayers are shown in Figs. S8-9. The variations of q_t^{max} and q_t^{min} with twist angle θ for graphene bilayers under various electric fields are shown in Fig. 2a and Fig. S10, respectively. These curves display a nonmonotonic variation profile, featuring distinct minima located at θ = 7.3°, 29.957° and 46.8°, respectively. Notably, the top layer of the 7.3°-twisted bilayer possesses the lowest q_t^{max} and q_t^{min}, while that of the AB-stacked bilayer (θ = 0°) possesses the highest q_t^{max} and q_t^{min}. The application of an electric field to these bilayers increases both q_t^{max} and q_t^{min}, yet the increased magnitude in twisted bilayers is smaller than that in AB-stacked bilayers. Furthermore, the maximum charge changes Δq_t^{max} ($\Delta q_t^{max} = q_t^{max} - q_t^{min}$) during interlayer sliding were calculated both in the absence of and under electric fields. As shown in Fig. 2b, the variations of Δq_t^{max} with θ also display a nonmonotonic variation profile, and the electric field exerts a weaker influence on Δq_t^{max} for twisted bilayers compared to AB-stacked bilayers. Then the difference in Δq_t^{max} between no electric field and under a 2 V/nm field, defined as $(\Delta q_t^{max})_2 - (\Delta q_t^{max})_0$ with the subscript denoting the field strength, was calculated for these graphene bilayers. As shown in Fig. 2c, the 7.3°-twisted bilayer exhibits the smallest value of $(\Delta q_t^{max})_2 - (\Delta q_t^{max})_0$ (0.42 nC/mm^2), which is one order of magnitude lower than that (1.27 nC/mm^2) of the AB-stacked bilayer. This indicates that interlayer charge transfer induced in twisted graphene bilayers by interlayer sliding are insensitive to applied electric fields for certain twisted bilayers such as those with twist angles of 7.3°, 29.957° and 46.8°.

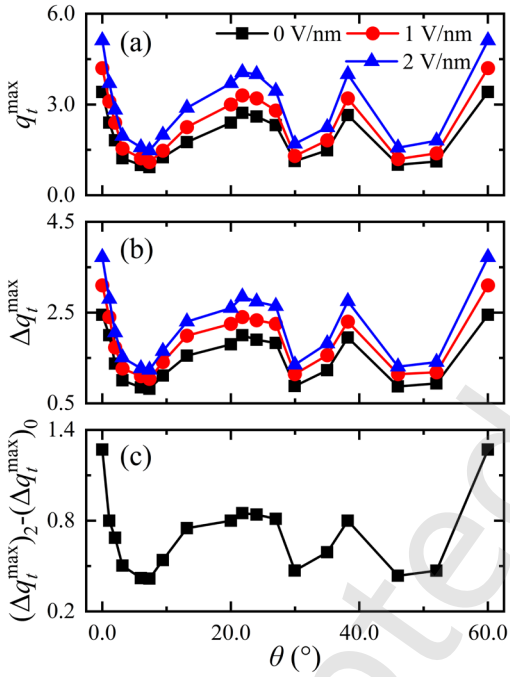

Fig. 2 Variations of ML-predicted (a) q_t^{max}, (b) Δq_t^{max} and (c) $(\Delta q_t^{max})_2 - (\Delta q_t^{max})_0$ (in units of nC/mm^2) with the twist angle θ of graphene bilayers under various electric fields.

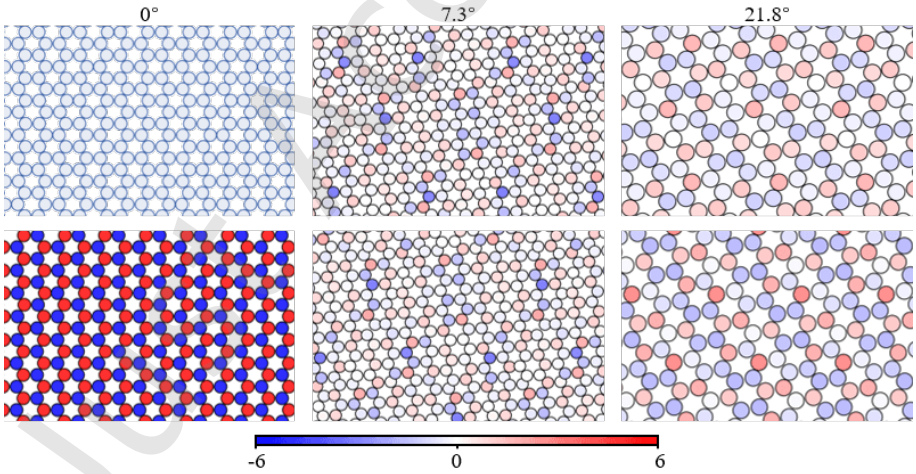

Fig. 3 Contour plots of ML-predicted Bader charge deviations Δq_i (in units of 10^{-2} e) for the top layers of AB-stacked, 7.3°-twisted and 21.8°-twisted graphene bilayers at the q_t^{min} (top) and q_t^{max} (bottom) stacking positions under a 2 V/nm electric field.

To better elucidate the field influence on the charge distribution in twisted graphene bilayers, the contours plots of the Δq_i of C atoms in the top layers at the q_t^{min} and q_t^{max} stacking positions under a field of 2 V/nm and without field are shown in Fig. 3 and Fig. S11, respectively. Compared to the

homogeneous charge distribution observed in the top layer of the AB-stacked bilayer, the top layers of the twisted bilayers exhibit a spatially heterogeneous charge distribution. In the presence of a field of 2 V/nm, the charge distribution in the top layer of the AB-stacked bilayer at the q_t^{min} stacking position is markedly different from that at the q_t^{max} stacking position. In contrast, the difference in the heterogeneous charge distribution between the q_t^{min} and q_t^{max} stacking positions is relatively small for twisted bilayers. Among all twisted bilayers examined, the 7.3-twisted bilayer exhibits the smallest variation in interlayer sliding-induced charge redistribution and the weakest electric field-induced modulation on the charge deviations Δq_i. Moreover, the charge density differences of the top or bottom layers ρ_{diff} ($\rho_{diff} = \rho_{bilayer}^{top/bottom} - \rho_{monolayer}$, where $\rho_{bilayer}^{top/bottom}$ is the charge density of the top or bottom layer of a graphene bilayer, and $\rho_{monolayer}$ is the charge density of the top or bottom monolayer) at the q_t^{min} and q_t^{max} stacking positions without field and under a field of 2 V/nm are shown in Figs. S12-15. During interlayer sliding, the electric field-induced charge transfer and redistribution occurring at AB-stacked graphene bilayers are significantly stronger than those observed in twisted graphene bilayers.

The C atoms in graphene were typically assumed to be electrically neutral in most previous theoretical simulations about friction at graphene-graphene interfaces, with only vdW interactions between C atoms considered and no inclusion of electrostatic (Coulomb) interactions. To more accurately account for the interlayer interactions in graphene bilayers, we incorporated Coulomb interactions by assigning the ML-predicted Bader charge deviations Δq_i as effective atomic charges to the C atoms at different stacking positions, where positive Δq_i values correspond to positive charges, and negative values to negative charges. Coulomb interactions were then computed using the Coulomb pair style in conjunction with the particle-particle particle-mesh (PPPM) solver. Subsequently, the initial structures of the AB-stacked and twisted bilayers were relaxed again using the AIREBO potential, with vdW and Coulomb interactions explicitly included. The derived equilibrium interlayer distances of these bilayers differ slightly from those obtained by DFT calculations, as shown in Fig.

S4, further demonstrating the validity of the employed ML model. Based on the interlayer vdW interaction energies E_{vdW} calculated by the LJ potential and Coulomb interaction energies E_{coul} by the ML-predicted charges, the total interlayer interaction energies E_t ($E_t = E_{vdW} + E_{coul}$) of these graphene bilayers both in the absence and presence of electric fields were calculated for the 81 stacking positions, and the resulting energy surfaces for interlayer sliding are shown in Figs. S16-18. Then, the maximum energy barriers for interlayer sliding, denoted as ΔE_{max}, were calculated by $\Delta E_{\max} = E_{\mathrm{t}}^{max} - E_{\mathrm{t}}^{min}$, where E_{t}^{max} and E_{t}^{min} are the maximum and minimum interlayer interaction energies, respectively. It should be noted that the stacking positions corresponding to E_{t}^{max} and E_{t}^{min} do not fully coincide with those corresponding to q_t^{max} and q_t^{min}, see Table S3. This discrepancy arises from the heterogeneous charge distribution inherent to twisted graphene bilayers. Fig. 4a shows the variations of ΔE_{max} with the twist angle θ of graphene bilayers under different electric fields, and the variations of the maximum vdW and Coulomb energy barriers are shown in Fig. S19. The field-induced increase in ΔE_{max} originates from the interlayer Coulomb interaction change. It can be seen from Fig. 4a and Fig. S20 that the response of maximum interlayer sliding energy barrier and shear strength τ_{max} ($\tau_{\max} = \Delta E_{\max}/\Delta r$, where Δr is the displacement along the pathway from the E_{t}^{min} stacking state to the E_{t}^{max} stacking state) in twisted bilayers to applied electric fields is obviously weaker than that in an AB-stacked bilayer. The smallest electric-field-induced modulations of both ΔE_{max} and τ_{max} are observed in the 7.3°-twisted bilayer. Under a field of 2 V/nm, the values of $(\Delta E_{max})_2$ and $(\tau_{max})_2$ of the 7.3°-twisted bilayer are 3.82 meV/Å^2 and 1.33 MPa, respectively, falling within the ultralow friction regime [30], and the corresponding $(\Delta E_{max})_2$ - $(\Delta E_{max})_0$ and $(\Delta \tau_{max})_2$ - $(\Delta \tau_{max})_0$ are only 0.97 meV/Å^2 and 0.41 MPa, respectively. Meanwhile, the values of $(\Delta E_{max})_2$ and $(\Delta \tau_{max})_2$ of the AB-stacked bilayer are 22.99 meV/Å^2 and 35.86 MPa, respectively, and the corresponding $(\Delta E_{max})_2$ - $(\Delta E_{max})_0$ and $(\Delta \tau_{max})_2$ - $(\Delta \tau_{max})_0$ are 5.82 meV/Å^2 and 10.89 MPa, respectively. These values are one order of magnitude higher than those of the 7.3°-twisted bilayer. Therefore, interlayer friction in certain twisted bilayers (such as $\theta =$

7.3°, 29.957° and 46.8°) is insensitive to applied electric fields, enabling these systems to sustain ultralow interlayer friction even under extreme bias conditions.

Furthermore, we have directly computed the Bader charge deviations Δq_i of C atoms in the bilayers with twist angles of 0°, 7.3°, and 21.8° relative to those of C atoms in free-standing monolayers both in the absence of an electric field and under a vertical field of 2 V/nm, by using the DFT calculations. As shown in Table S4 and Table S5, the maximum charge change Δq_t^{max} between the DFT-derived q_t^{max} and q_t^{min} is smallest for the 7.3°-twisted bilayer. Under a field of 2 V/nm, the value of Δq_t^{max} (0.91 nC/mm^2) is in reasonable agreement with that of the corresponding ML-derived Δq_t^{max} (1.24 nC/mm^2). Moreover, the influence of the applied 2V/nm electric field of on the differences in the DFT-derived energy gap ΔE_{g}, interlayer electrostatic energy ΔE_{ES}, vdW energy ΔE_{vdW} and exchange-correlation energy ΔE_{XC} between the E_{t}^{max} and E_{t}^{min} stacking positions is weakest for the 7.3°-twisted bilayer, as shown in Fig. 4b and Figs. S21-23. Similar variations of ML-predicted ΔE_{max} and DFT-derived ΔE_{g} between the q_{t}^{max} and q_{t}^{min} stacking positions are observed for AB-stacked and twisted bilayers, as shown in Fig. S24. The slight change in the electronic structure of the 7.3°-twisted bilayer under a 2 V/nm electric field is consistent with its electric field-insensitive heterogeneous charge distribution and interlayer friction.

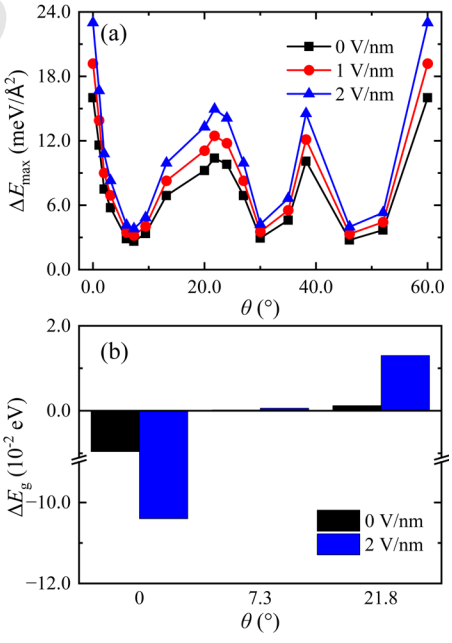

Fig. 4 (a) Variations of ML-predicted maximum sliding energy barriers $\Delta E_{\max}$ with the twist angle θ of graphene bilayers under various electric fields. (b) Differences in DFT-derived band gap ΔE_{g} of AB-stacked, 7.3°-twisted and 21.8°-twisted graphene bilayers between the E_{t}^{max} and E_{t}^{min} stacking positions in the absence and presence of a 2 V/nm electric field**.**

The Registry Index (RI) model [31,32] provides a geometrically intuitive and computationally efficient measurement for quantifying the interlayer stacking registry in layered material interfaces under interlayer sliding conditions, serving as a compelling tool for characterizing commensurability-related interfacial phenomena. An external electric field induces interlayer charge transfer and exchange in graphene bilayers, resulting in distinct atomic charges on the C atoms. Consequently, the existing RI model, which relies on a fixed atomic radius, is insufficient for effectively capturing field-induced interlayer registry change in graphene bilayers. Here, we have developed the RI method by introducing the ML-derived Bader charge deviation Δq_i of each C atom as a correction parameter for its atomic radius, thereby establishing a charge-modified RI model (RI_{CM}) for a graphene bilayer: $RI_{\mathrm{CM}} = \frac{S_{\mathrm{CC}} - S_{\mathrm{CC}}^{\min}}{S_{\mathrm{CC}}^{\max} - S_{\mathrm{CC}}^{\min}}$ with $r_i = \frac{4 - \Delta q_i}{4} \times r_0$. Where r_i is the charge-modified atomic radius of a C atom, r_0 ($r_0 = 0.71$ Å) is the reference C atomic radius [31,32], S_{CC} represents the sum of pairwise projection overlaps between all atoms in the top layer and those in the bottom layer, while $S_{\mathrm{CC}}^{\max}$ and $S_{\mathrm{CC}}^{\min}$ (corresponding to the AA stacking and AB stacking, respectively) denote the global maximum and minimum overlap sums, respectively. Figure S25 shows the RI_{CM} values of AB-stacked and twisted graphene bilayers for interlayer sliding without electric field and under a 2 V/nm field. Applying an electric field enhances the overlap between the top and bottom layers, as field-induced interlayer charge transfer modulates the atomic radii. For twisted bilayers, the maximum RI_{CM} corresponds to the q_t^{max} stacking position, whereas the minimum RI_{CM} corresponds to the q_t^{min} stacking positions, see Table S3. In contrast**,** for the AB-stacked graphene bilayer, the maximum RI_{CM} corresponds to the q_t^{min} stacking position, whereas the minimum RI_{CM} corresponds to the q_t^{max} stacking positions.

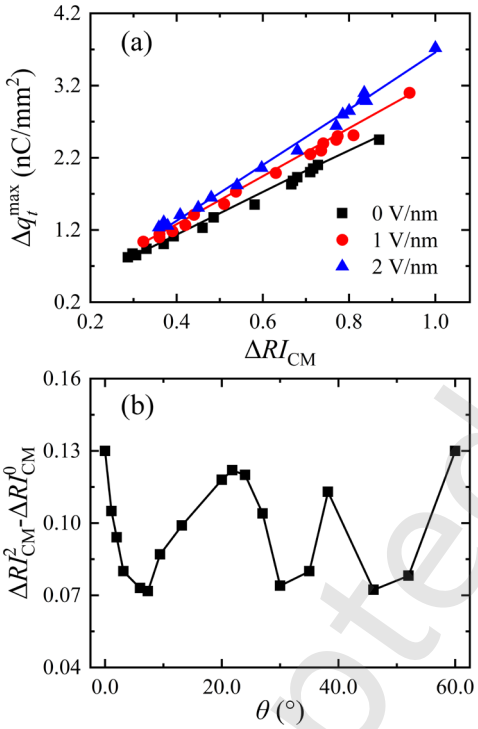

Fig. 5 (a) Variations of Δq_t^{max} with the ΔRI_{CM} of graphene bilayers under various electric fields. (b) Variations of $\Delta RI^2_{\mathrm{CM}} - \Delta RI^0_{\mathrm{CM}}$ with the twist angle θ of graphene bilayers.

Furthermore, the maximum change in the RI_{CM} values between the q_t^{max} and q_t^{min} stacking positions was calculated by $\Delta RI_{\mathrm{CM}} = RI_{\mathrm{CM}}^{\max} - RI_{\mathrm{CM}}^{\min}$, and the variations of ΔRI_{CM} with twist angle θ under various electric fields are shown in Fig. S26. These curves also display a nonmonotonic variation profile, with distinct minima occurring at θ = 7.3°, 29.957° and 46.8°. A smaller ΔRI_{CM} means lower interlayer friction [32]. Among them, the 7.3°-twisted bilayer exhibits the lowest ΔRI_{CM} value. As the electric field strength increases, the ΔRI_{CM} value monotonically increases but eventually approaches a saturation limit in which the atomic radius of all C atoms is fixed at r_0 = 0.71 Å. To further reveal the relation of ΔRI_{CM} with charge transfer in graphene bilayers, Figure 5a shows the variations of the ML-derived maximum charge change Δq_t^{max} with ΔRI_{CM} under various electric fields. As clearly shown, Δq_t^{max} exhibits an approximately linear dependence on ΔRI_{CM}. The variation curves can be fitted by the equation $(\Delta q_t^{max})_k = A_k \Delta RI^k_{\mathrm{CM}} + B_k$ (k = 0,1 or 2), with k denoting the strength of the applied electric field, and A and B representing the corresponding fitting parameters, as given in Table S6. The

value of A is positive and increases with increasing the field strength. This means that, under a stronger electric field, an identical increment in $\Delta RI_{\mathrm{CM}}^{k}$ results in a greater increase in $(\Delta q_t^{max})_k$. The parameter B quantifies the interlayer charge transfer under the idealized assumption that the interlayer overlapping area of a twisted bilayer graphene remains invariant during interlayer sliding. For a graphene bilayer under an electric field, the difference between its $(\Delta q_t^{max})_k$ and $(\Delta q_t^{max})_0$ is $(\Delta q_t^{max})_k - (\Delta q_t^{max})_0 = (A_k - A_0)(\Delta RI_{\mathrm{CM}}^{2} - \Delta RI_{\mathrm{CM}}^{0}) + (B_k - B_0)$. As A_k is always larger than A_0, the value of $(\Delta q_t^{max})_k - (\Delta q_t^{max})_0$ increases monotonically with $\Delta RI_{\mathrm{CM}}^{k} - \Delta RI_{\mathrm{CM}}^{0}$. Therefore, the electric field-induced interlayer charge transfer and redistribution in a graphene bilayer during interlayer sliding can be fundamentally described and governed by the magnitude of $\Delta RI_{\mathrm{CM}}^{k} - \Delta RI_{\mathrm{CM}}^{0}$. For certain twisted bilayers such as those with twist angles of θ = 7.3°, 29.957° and 46.8°, see Fig. 5b, the difference $\Delta RI_{\mathrm{CM}}^{k} - \Delta RI_{\mathrm{CM}}^{0}$ is significantly smaller than that of an AB-stacked bilayer due to a slight interlayer charge transfer, resulting in robust insensitivity to applied electric fields. The value of $\Delta RI_{\mathrm{CM}}^{k} - \Delta RI_{\mathrm{CM}}^{0}$ can be used as a concise and physically interpretable descriptor for designing low-friction interfaces in electrically gated graphene devices.

Moreover, we have conducted additional calculations for AB-stacked, 7.3°-twisted and 21.8°-twisted graphene bilayers by combining the KC potential [33] for interlayer vdW interactions and ML-predicted charge deviations for Coulomb interactions. As shown in Figure S27, the total energy surfaces derived by both the KC+ML and LJ+ML models exhibit excellent agreement with those obtained from the DFT-derived energy surfaces. Furthermore, the differences in the total energy surfaces obtained from the KC+ML and LJ+ML models for graphene bilayers with twist angles of 2.1°, 3.2°, and 27.8° are slight, as shown in Figure S28. These results indicate that the LJ+ML model sufficiently captures the essential features of interlayer interactions in twisted graphene bilayers and that interlayer Coulomb interactions play a key role in shaping the total energy surface during interlayer sliding.

4 Conclusions

In summary, our comprehensive DFT-based ML study reveals that heterogeneous charge distribution and interlayer sliding-induced charge transfer in certain twisted graphene bilayers, particularly those with twist angles of 7.3°, 29.957° and 46.8°, are robustly insensitive to applied vertical electric fields compared to the AB-stacked bilayer. This field insensitivity enables such twisted bilayers to maintain ultra-low interlayer friction and exhibit a slight energy gap change during interlayer sliding, even under a strong electric field of 2 V/nm. A charge-modified RI_{CM} model has been developed for graphene bilayers to quantitatively describe the coupling effect of interlayer sliding and electric fields on their interlayer charge transfer and exchange. The maximum charge change difference $(\Delta q_t^{max})_k - (\Delta q_t^{max})_0$ in the graphene layers between biased and unbiased conditions linearly increases with the corresponding maximum registry index change difference $\Delta RI_{\mathrm{CM}}^k - \Delta RI_{\mathrm{CM}}^0$. A smaller value of $\Delta RI_{\mathrm{CM}}^k - \Delta RI_{\mathrm{CM}}^0$ indicates a weaker response and stronger insensitivity to electric fields. The DFT-based ML results, combined with the charge-modified registry index model, deepen our fundamental understanding of the coupled effect of interlayer sliding and external electric fields in twisted graphene bilayers and provide valuable insights for achieving ultralow interface friction under extreme bias conditions.

Acknowledgements

This work is supported and funded by the National Natural Science Foundation of China (12472105), Basic Research Program of Jiangsu (BK20252024), Research Fund of State Key Laboratory of Mechanics and Control for Aerospace Structures (Nanjing University of Aeronautics and Astronautics, Grant No. MCAS-I-0525K01), and a Project Funded by the Priority Academic Program Development of Jiangsu Higher Education Institutions.

Author contributions

Hao Li: data curation, formal analysis, investigation, methodology, software, validation, visualization, writing – original draft; Wanlin Guo: supervision; Yufeng Guo: conceptualization, methodology, writing - review & editing, supervision, funding acquisition.

Availability of data and materials

The data that support the findings of this study is available from the corresponding author upon reasonable request."

Competing interests

The authors have no competing interests to declare that are relevant to the content of this article.

Electronic Supplementary Material: Supplementary material

Details of the ML technique and settings; table showing unit cell sizes, stacking positions, comparison of q_t^{min}, q_t^{max} and Δq_t^{max} between the ML prediction and DFT calculations, fitting parameters; figures showing configurations of AB-stacked and twisted graphene bilayers, ML details under different electric fields, variations of equilibrium interlayer distances, total charge deviation surfaces, stacking configurations corresponding to the q_t^{min} and q_t^{max} stacking position, variations of ML-predicted q_t^{min}, contours of ML-predicted Bader charge deviations without electric field, charge density differences for the top and bottom layers, energy surfaces, variations of ML-predicted maximum sliding vdW energy barriers, Coulomb energy barriers and shear strength $\tau_{\max}$, variations of ML-predicted $\Delta E_{\max}$ and DFT-derived ΔE_{g} between q_{t}^{max} and q_{t}^{min}, DFT-derived Δq_t^{max}, differences in DFT-derived ΔE_{ES}, ΔE_{vdW} and ΔE_{XC}, band gaps, RI_{CM} surfaces of AB-stacked and twisted graphene bilayers, Variations of ΔRI_{CM}, comparison between the KC+ML and LJ+ML models.

References

[1]. Seiler A M, Geisenhof F R, Winterer F, Watanabe K, Taniguchi T, Xu T, Zhang F, Weitz R T. Quantum cascade of correlated phases in trigonally warped bilayer graphene. *Nature* **608**(7922): 298–302 (2022).

[2]. Zhang Y, Shavit G, Ma H, Han Y, Siu C W, Mukherjee A, Watanabe K, Taniguchi T, Hsieh D, Lewandowski C, Von Oppen F, Oreg Y, Nadj-Perge S. Twist-programmable superconductivity in spin–orbit-coupled bilayer graphene. *Nature* **641**(8063): 625–631 (2025).

[3]. Lee J, Chiu H-Y, Zhao L, Shan J, Feng P X-L. Temperature compensated graphene nanomechanical resonators. *Adv Funct Mater.* **35**(24): 2415708 (2025).

[4]. Cao Y, Fatemi V, Fang S, Watanabe K, Taniguchi T, Kaxiras E, Jarillo-Herrero P. Unconventional superconductivity in magic-angle graphene superlattices. *Nature* **556**(7699): 43–50 (2018).

[5]. Cao Y, Fatemi V, Demir A, Fang S, Tomarken S L, Luo J Y, Sanchez-Yamagishi J D, Watanabe K, Taniguchi T, Kaxiras E, Ashoori R C, Jarillo-Herrero P. Correlated insulator behaviour at half-filling in magic-angle graphene superlattices. *Nature* **556**(7699): 80–84 (2018).

[6]. Yankowitz M, Chen S, Polshyn H, Zhang Y, Watanabe K, Taniguchi T, Graf D, Young A F, Dean C R. Tuning superconductivity in twisted bilayer graphene. *Science* **363**(6431): 1059–1064 (2019).

[7]. Lu X, Stepanov P, Yang W, Xie M, Aamir M A, Das I, Urgell C, Watanabe K, Taniguchi T, Zhang G. Superconductors, orbital magnets and correlated states in magic-angle bilayer graphene. *Nature* **574**(7780): 653–657 (2019).

[8]. Wong D, Nuckolls K P, Oh M, Lian B, Xie Y, Jeon S, Watanabe K, Taniguchi T, Bernevig B A, Yazdani A. Cascade of electronic transitions in magic-angle twisted bilayer graphene. *Nature* **582**(7811): 198–202 (2020).

[9]. Minkin A S, Lebedeva I V, Popov A M, Vyrko S A, Poklonski N A, Lozovik Y E. Restriction of macroscopic structural superlubricity due to structure relaxation by the example of twisted graphene bilayer. *Phy. Rev Mater* **9**(2): 024002 (2025).

[10]. Dienwiebel M, Verhoeven G S, Pradeep N, Frenken J W, Heimberg J A, Zandbergen H W.

Superlubricity of graphite. *Phys Rev Lett* **92**(12): 126101 (2004).

[11]. Guo Y, Guo W, Chen C. Tuning field-induced energy gap of bilayer graphene via interlayer spacing. *Appl Phys Lett* **92**(24): 243101 (2008).

[12]. Li C, Xu F, Li B, Li J, Li G, Watanabe K, Taniguchi T, Tong B, Shen J, Lu L. Tunable superconductivity in electron-and hole-doped bernal bilayer graphene. *Nature* **631**(8020): 300–306 (2024).

[13]. Yeh C-H, Lin Y-C, Chen Y-C, Lu C-C, Liu Z, Suenaga K, Chiu P-W. Gating Electron–Hole Asymmetry in Twisted Bilayer Graphene. *ACS Nano* **8**(7): 6962–6969 (2014).

[14]. Dutta R, Ghosh A, Mandal S, Watanabe K, Taniguchi T, Krishnamurthy H R, Banerjee S, Jain M, Das A. Electric Field-Tunable Superconductivity with Competing Orders in Twisted Bilayer Graphene near the Magic Angle. *ACS Nano* **19**(5): 5353–5362 (2025).

[15]. Wang J, Li J, Li C, Cai X, Zhu W, Jia Y. Tuning the nanofriction between two graphene layers by external electric fields: a density functional theory study. *Tribol Lett* **61**(1): 4 (2016).

[16]. Song A, Shi R, Lu H, Wang X, Hu Y, Gao H-J, Luo J, Ma T. Fluctuation of interfacial electronic properties induces friction tuning under an electric field. *Nano Lett* **22**(5): 1889–1896 (2022).

[17]. Kresse G, Furthmüller J. Efficiency of ab-initio total energy calculations for metals and semiconductors using a plane-wave basis set. *Comput Mater Sci* **6**: 15 (1996).

[18]. Kresse G, Furthmüller J. Efficient iterative schemes for *ab initio* total-energy calculations using a plane-wave basis set. *Phys Rev B* **54**(16): 11169–11186 (1996).

[19]. Perdew J P, Burke K, Ernzerhof M. Generalized gradient approximation made simple. *Phys Rev Lett* **77**: 3865 (1996).

[20]. Blöchl P E. Projector augmented-wave method. *Phys Rev B* **50**: 17953 (1994).

[21]. Murray É D, Kong L, Lundqvist B I, Langreth D C, Lee K. Higher-accuracy van der waals density functional. *Phys Rev B* **82**: 81101 (2010).

[22]. Huang P, Guo D, Xie G, Li J. Softened mechanical properties of graphene induced by electric

field. *Nano Lett* **17**(10): 6280–6286 (2017).

[23]. Chandrasekaran A, Kamal D, Batra R, Kim C, Chen L, Ramprasad R. Solving the electronic structure problem with machine learning. *npj Comput Mater* **5**: 22 (2019).

[24]. Abadi M, Agarwal A, Barham P, Brevdo E, Chen Z, Citro C, Corrado G S, Davis A, Dean J, Devin M. Tensorflow: large-scale machine learning on heterogeneous distributed systems. *Arxiv Prepr Arxiv:1603,04467* (2016).

[25]. Kingma D P, Ba J. Adam: a method for stochastic optimization. *Arxiv Prepr Arxiv:1412,6980* (2014).

[26]. LeCun Y, Bengio Y, Hinton G. Deep learning. *Nature* **521**(7553): 436 (2015).

[27]. Nair V, Hinton G E. Rectified linear units improve restricted boltzmann machines. *Proceedings of the 27th International Conference on Machine Learning (ICML-10)* 807–814 (2010).

[28]. Stuart S J, Tutein A B, Harrison J A. A reactive potential for hydrocarbons with intermolecular interactions. *J Chem Phys* **112**: 6472 (2000).

[29]. Bader R F. Atoms in molecules. *Acc Chem Res* **18**: 9 (1985).

[30]. Li J, Li J, Luo J. Superlubricity of graphite sliding against graphene nanoflake under ultrahigh contact pressure. *Adv Sci* **5**(11): 1800810 (2018).

[31]. Hod O. Interlayer commensurability and superlubricity in rigid layered materials. *Phys Rev B* **86**(7): 075444 (2012).

[32]. Guo Y, Qiu J, Guo W. Reduction of interfacial friction in commensurate graphene/h-BN heterostructures by surface functionalization. *Nanoscale* **8**(1): 575–580 (2016).

[33]. Kolmogorov A N, Crespi V H. Smoothest bearings: interlayer sliding in multiwalled carbon nanotubes. *Phys. Rev. Lett.* **85**: 4727 (2000).

Wanlin Guo. He received his Ph.D. from Northwestern Polytechnical University in solid mechanics. He is currently a full time professor and director in Institute of Nanoscience, Key Laboratory of Intelligent Nano Mechanics and Control for Mechanical Structures. Deputy director of State Key Laboratory of Mechanics and Control for Aerospace Structures in Nanjing University of Aeronautics and Astronautics. His researches focus on nanoscale physical mechanics, intelligent nanomaterials and devices, highly efficient energy transfer nanotechnology, three-dimensional fatigue fracture and damage tolerance and durability design of structures.

Yufeng Guo. He is a Professor in College of Aerospace Engineering, Nanjing University of Aeronautics and Astronautics. Dr. Guo received his Ph.D. degree in solid mechanics from Nanjing University of Aeronautics and Astronautics in 2006. His research focuses on multi-field coupling mechanism, properties and design of nanoscale functional devices and systems utilizing first-principles calculations, molecular dynamics simulations and mechanics modeling.

Hao Li. He is a Ph.D. candidate in College of Aerospace Engineering, Nanjing University of Aeronautics and Astronautics under the supervision of Prof. Yufeng Guo. His research interests include the friction behavior of low-dimensional materials and first-principles calculations.